J. Fluid Mech. (2001), *vol.* 447, *pp.* 357–375.
DOI: 10.1017/S0022112001006048 Printed in the United Kingdom

Linear internal waves and the control of stratified exchange flows

By A. McC. HOGG, K. B. WINTERS† AND G. N. IVEY

Centre for Water Research, University of Western Australia, Nedlands, Western Australia 6907, Australia

(Received 18 December 2000 and in revised form 17 May 2001)

Internal hydraulic theory is often used to describe idealized bi-directional exchange flow through a constricted channel. This approach is formally applicable to layered flows in which velocity and density are represented by discontinuous functions that are constant within discrete layers. The theory relies on the determination of flow conditions at points of hydraulic control, where long interfacial waves have zero phase speed. In this paper, we consider hydraulic control in continuously stratified exchange flows. Such flows occur, for example, in channels connecting stratified reservoirs and between homogeneous basins when interfacial mixing is significant. Our focus here is on the propagation characteristics of the gravest vertical-mode internal waves within a laterally contracting channel.

Two approaches are used to determine the behaviour of waves propagating through a steady, continuously sheared and stratified exchange flow. In the first, waves are mechanically excited at discrete locations within a numerically simulated bi-directional exchange flow and allowed to evolve under linear dynamics. These waves are then tracked in space and time to determine propagation speeds. A second approach, based on the stability theory of parallel shear flows and examination of solutions to a sixth-order eigenvalue problem, is used to interpret the direct excitation experiments. Two types of gravest mode eigensolutions are identified: *vorticity* modes, with eigenfunction maxima centred above and below the region of maximum density gradient, and *density* modes with maxima centred on the strongly stratified layer. Density modes have phase speeds that change sign within the channel and are analogous to the interfacial waves in hydraulic theory. Vorticity modes have finite propagation speed throughout the channel but undergo a transition in form: upwind of the transition point the vorticity mode is trapped in one layer. It is argued that modes trapped in one layer are not capable of communicating interfacial information, and therefore that the transition points are analogous to control points. The location of transition points are identified and used to generalize the notion of hydraulic control in continuously stratified flows.

1. Introduction

Internal hydraulic theory (see, for example, Wood 1968, 1970; Armi 1986) can be used to describe density-driven flows in which fluid motion is determined by a buoyancy and inertia force balance. In particular, inviscid flow through constricted

† Also at: Applied Physics Laboratory, University of Washington, Seattle, WA 98105, USA.

channels is the major application of hydraulic theory. If mixing and friction are negligible, the hydraulic solution can be used to calculate fluid velocity in distinct layers which interact in only a limited way. The velocities scale with the speed of interfacial waves and depend upon the depth of the interface.

The key to understanding hydraulic flows lies in the existence of control points. At a control point, the flow is constrained in that velocities are such that the phase speed of one of two interfacial waves is zero. The existence of control points has two major ramifications. First, given knowledge of the flow at the control points, it is possible to calculate global information about the flow field within a simple domain, provided the fundamental assumptions are correct. Secondly, since velocities are limited by internal wave speeds at the control points, hydraulic theory places an upper bound on the total flux through the channel, the quantity of paramount importance to estimating transport in geophysical systems.

It is often difficult to determine whether an exchange flow between two basins is hydraulically controlled. One reason for this is that hydraulic control is formally defined for layered flow, that is, horizontal flow with uniform velocity and density within discrete layers and discontinuities in these quantities between layers. In contrast, observed flows are continuously sheared and stratified. Though large gradients in velocity and density are often present, these finite-thickness interfaces may be displaced vertically from one another, making an approximate decomposition into layers difficult and subjective. Unfortunately, using the results of hydraulic theory to determine whether such flows are controlled depends sensitively on how one defines the layers (see, for example, Gregg & Özsoy 2001; Pratt *et al.* 1999). Furthermore, flux estimates based on layered hydraulic solutions are often significant overestimates of the true flux in continuously stratified flows (Winters & Seim 2000; Hogg, Ivey & Winters 2001).

Our objective here is to extend the notion of hydraulic control to continuously stratified flows in such a way that determining whether a flow is controlled and locating the position of control points can be done in an objective manner. To simplify the presentation we consider in detail the limited class of flows resulting from a classical lock-exchange problem for a fluid with non-negligible viscosity and diffusivity. In particular, we consider exchange flow through a laterally contracting channel separating two infinite basins filled initially with homogeneous fluid of different densities. For channels with slowly varying width, the solution in the inviscid, non-diffusive limit can be obtained using two-layer hydraulic theory as described in Armi (1986) and Lawrence (1990). When mixing and dissipation are significant, a finite-thickness interfacial layer is produced with the zero-isotach displaced from the position of the maximum density gradient.

Before considering the continuously stratified case, we briefly review the concept of hydraulic control in the idealized two-layer theory. Consider a flat-bottomed channel of length L and depth H, with a simple minimum width W as shown in figure 1(a), where spatial variables have already been non-dimensionalized by the size of the domain. At the left-hand end of the channel is an infinite reservoir of density ρ_1, and at the right-hand end of the channel is a similar reservoir with a higher density ρ_2. Assuming that viscosity and mixing are negligible, and that the width of the channel varies slowly with horizontal distance, fluid velocities in two discrete layers will be constant within the layer, and approximately horizontal. Under these assumptions, a simple model based on conservation of mass within each of the two layers in combination with conservation of energy (Bernoulli's equation) captures the nonlinear dynamics of exchange flow in the system (see, for example Wood 1970;

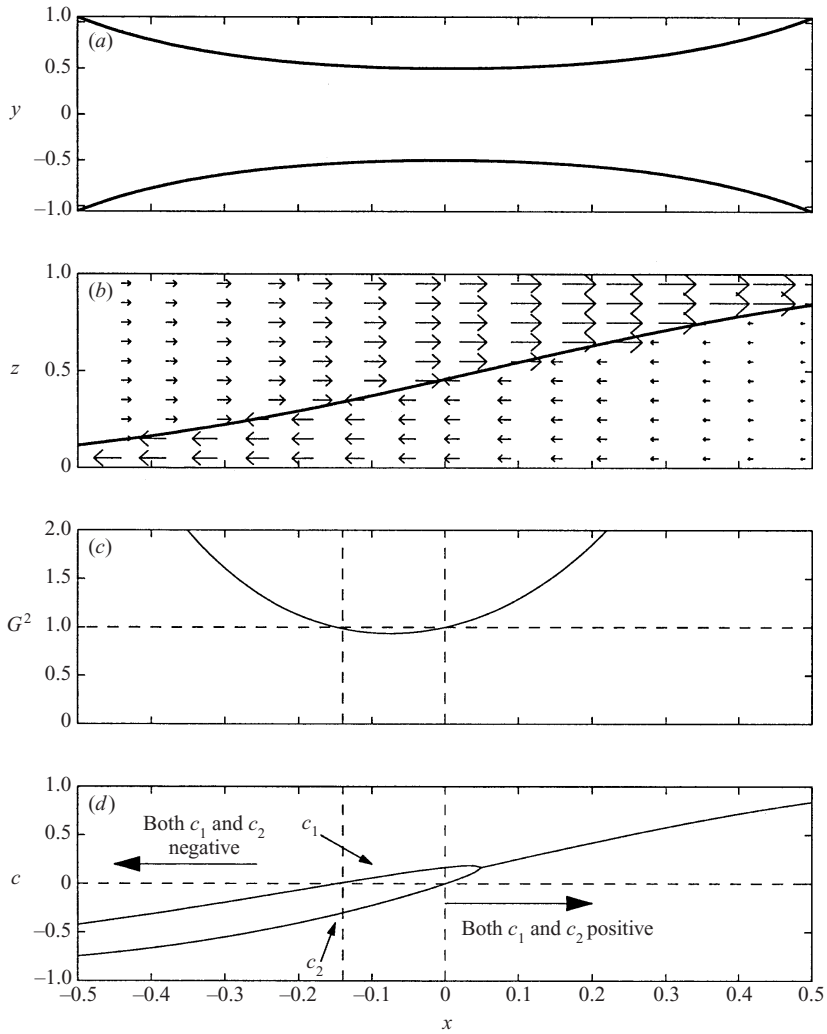

FIGURE 1. Characteristics of the hydraulic solution with $q_r = 2$. (*a*) Channel in plan view; (*b*) layer height and velocity vectors in elevation view; (*c*) variation of the composite Froude number G^2; (*d*) plot of wave speeds.

Armi 1986; Armi & Farmer 1986, Lawrence 1990; Baines 1995). The resulting flow is shown in figure 1(*b*).

Points of control occur when the composite Froude number,

$$G^2 \equiv \frac{u_1^2}{h_1} + \frac{u_2^2}{h_2} - \frac{(1-r)u_1^2u_2^2}{h_1h_2} = 1, \tag{1.1}$$

where h_i is the dimensionless depth of each layer (non-dimensionalized by H), and u_i the dimensionless velocity (normalized by the inviscid wave speed $(g'H)^{1/2}$). The ratio of layer densities is $r \equiv \rho_1/\rho_2$, and $g' = g(1-r)$ is the reduced gravity. As shown by the variation of G^2 with x in figure 1(*c*), in the case where the channel has a simple width minimum and a controlled flow has a net barotropic component (defined by the ratio of layer fluxes $q_r = q_1/q_2$), there are two points of control. A topographic control is located at the width minimum ($x = 0$ in figure 1) and a virtual control is

located upstream of the width minimum with respect to the barotropic flow direction ($x \approx -0.13$). Between these two points, the flow is said to be subcritical while the flow between the reservoirs and the control points is said to be supercritical. We are ignoring here the possibility of hydraulic jumps as they do not formally appear in the theory.

It can be shown (Dalziel 1991; Baines 1995) that for a two-layer flow the hydraulic control condition can be written

$$G^2 = 1 + \frac{c_1 c_2}{h_1 h_2} = 1, \tag{1.2}$$

where c_1 and c_2 are the phase speeds of the two interfacial waves non-dimensionalized by $(g'H)^{1/2}$. In a quiescent fluid, we expect two interfacial waves to exist: one travelling to the right, and one to the left. When the layers flow in opposite directions, (1.2) implies that at least one wave is arrested at a point of hydraulic control. This is demonstrated in figure 1(*d*), where normalized waves speeds are plotted as a function of x. In subcritical flow, $G^2 < 1$ and the two waves travel in opposite directions. In supercritical flow, $G^2 > 1$ and both waves propagate in the same direction, away from the contraction and toward one of the reservoirs. A central region of subcritical flow is said to be insulated from interface disturbances in either basin in the sense that such changes cannot be communicated to the subcritical region via long interfacial internal waves. In this way, changes can occur in the reservoirs which do not alter the flux through the channel.

The two long-wave speeds coalesce downstream of the contraction (relative to the fastest flowing layer). Mathematically, this means that the wave speeds are complex, implying that the modes are unstable there. This aspect of the hydraulic solution is described by Lawrence (1990) who introduces a stability Froude number. The implication is that hydraulic theory is not self-consistent: instabilities will be generated in part of the domain leading to mixing of density and momentum between the two layers which violates the fundamental assumptions. Nonetheless, numerical simulations have demonstrated that weak damping suppresses long-wave instabilities (Winters & Seim 2000), and that the hydraulic solution is a good approximation to modelled flows in the limit of weak damping (Hogg *et al.* 2001).

Hydraulic control of a multi-layered exchange flow is investigated by Engqvist (1996). By defining two groups of layers, each group flowing in the opposite direction, with a stagnant layer in between, it is possible to calculate the position of a topographic control and a number of virtual controls. An extra virtual control is formed for each extra layer and the virtual controls refer to points at which the higher vertical modes become critical. In this case the flow is still controlled by the lowest mode. The multi-layered technique is useful for conditions where end reservoirs are stratified, but the condition that groups of layers are decoupled prevents the application of this technique to flows where mixing is significant.

In this paper we consider the propagation of internal waves in a flow similar to the two-layer solution discussed above but where mixing and dissipation have acted to smooth the discontinuities between layers producing a continuously sheared and stratified exchange flow. A steady-state exchange flow is generated through direct simulation of a lock-exchange problem with finite mixing and dissipation. The simulation is run to a quasi-steady state, at which point it is averaged with respect to the cross-channel coordinate to produce a background flow field $\bar{u}(x,z)$, $\bar{w}(x,z)$ and $\bar{\rho}(x,z)$. Two complementary techniques are then used to quantify the propagation characteristics of linear internal waves through this background flow.

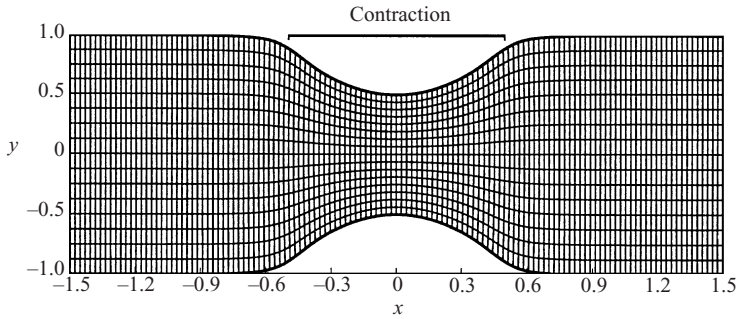

FIGURE 2. Graph of channel shape and curvilinear coordinates in plan view.

First, we modify the computational model to directly simulate the evolution of spatially localized disturbances and determine the speed and direction of the excited waves as a function of position within the channel. We then consider the eigenvalue problem for parallel shear flow at different locations within the channel, allowing for the effects of viscosity and diffusivity. We limit our discussion to the gravest vertical modes, noting that additional modes appear in the continuously sheared and stratified case. We do not consider issues related to higher vertical modes. The results of these two sets of experiments are then used to examine the hydraulic control of the underlying flow.

2. Numerical experiments

2.1. *Numerical simulation of exchange flows*

The numerical experiments in this study are based on a three-dimensional model called S-FIT (Winters, Seim & Finnigan 2000) which solves the fluid equations of motion in a curvilinear coordinate system. The coordinates are orthogonal, however the boundary can be distorted in one dimension as shown in figure 2 to simulate flow down a channel of varying width. The domain shown in figure 2 is used for all numerical experiments described here.

S-FIT solves the following equations:

$$\frac{\partial \boldsymbol{u}}{\partial t} + \boldsymbol{u}\cdot\nabla\boldsymbol{u} = -\frac{1}{\rho_0}\nabla p - \frac{\hat{\boldsymbol{z}} g\rho}{\rho_0} + \nabla\cdot K\nabla\boldsymbol{u}, \tag{2.1}$$

$$\frac{\partial \rho}{\partial t} + \boldsymbol{u}\cdot\nabla\rho = \nabla\cdot K\nabla\rho, \tag{2.2}$$

$$\nabla\cdot\boldsymbol{u} = 0, \tag{2.3}$$

where $\boldsymbol{u} = (u, v, w)$ is the velocity vector, ρ is the density and p the pressure. In addition, we define reference density ρ_0, a turbulent eddy viscosity K, and assume a turbulent Prandtl number of one, so that K also represents turbulent eddy diffusivity. Note that K is dimensionless (normalized by $(g'H^3)^{1/2}$). Usually, turbulent parameters such as eddy viscosity and eddy diffusivity are calculated explicitly by a closure scheme (see Winters & Seim 2000). We represent the effect of such mixing only crudely here and prescribe a constant eddy viscosity/diffusivity throughout the contraction region, as discussed in Hogg *et al.* (2001). The purpose here is to generate a continuously sheared and stratified flow similar to that expected if strong mixing were to occur.

The flows simulated are identical to the flow detailed by Hogg *et al.* (2001). The

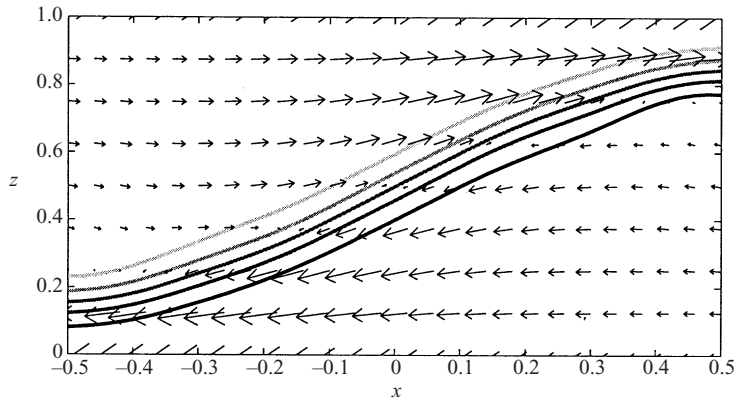

FIGURE 3. Numerical simulation of exchange flow showing isopycnals and velocity vectors in elevation view.

surface is a fixed lid, with free-slip conditions on upper, lower and sidewall boundaries. The streamwise end conditions are that inflowing density is specified (representing infinite homogeneous reservoirs), and a surface pressure difference across the length of the channel is imposed. The channel is $120 \times 10 \times 10\,\mathrm{m}$, and has $129 \times 17 \times 65$ gridpoints. The resulting base flow, for $K \approx 10^{-3}$ and $q_r \approx 1$ can be seen in figure 3 with velocity vectors and selected isopycnals shown.

2.2. *Direct excitation experiments*

We use a slightly adapted version of S-FIT to look at the evolution of linear perturbations in a steady-state flow. Starting with (2.1)–(2.3), assume that the steady-state solution satisfies these equations in our curvilinear domain. Each variable is then separated into two parts: a perturbation quantity (prime) and a background steady state (overbar), by writing

$$\boldsymbol{u}(x,y,z,t) = \bar{\boldsymbol{u}}(x,z) + \boldsymbol{u}'(x,y,z,t), \tag{2.4}$$

$$\rho(x,y,z,t) = \bar{\rho}(x,z) + \rho'(x,y,z,t), \tag{2.5}$$

$$p(x,y,z,t) = \bar{p}(x,z) + p'(x,y,z,t). \tag{2.6}$$

This is substituted into (2.1)–(2.3), to give

$$\frac{\partial \boldsymbol{u}'}{\partial t} + \boldsymbol{u}'\cdot\nabla\boldsymbol{u}' + \boldsymbol{u}'\cdot\nabla\bar{\boldsymbol{u}} + \bar{\boldsymbol{u}}\cdot\nabla\boldsymbol{u}' = -\frac{1}{\rho_0}\nabla p' - \frac{\hat{\boldsymbol{z}}g\rho'}{\rho_0} + \nabla\cdot K\nabla\boldsymbol{u}', \tag{2.7}$$

$$\frac{\partial \rho'}{\partial t} + \boldsymbol{u}'\cdot\nabla\bar{\rho} + \bar{\boldsymbol{u}}\cdot\nabla\rho' + \boldsymbol{u}'\cdot\nabla\rho' = \nabla\cdot K\nabla\rho', \tag{2.8}$$

$$\nabla\cdot\boldsymbol{u}' = 0, \tag{2.9}$$

where we have removed background variables which independently satisfy (2.1)–(2.3). Since we are interested in the linear evolution of these perturbations, we remove the possibility of nonlinear interactions by eliminating double perturbation quantities, giving

$$\frac{\partial \boldsymbol{u}'}{\partial t} + \boldsymbol{u}'\cdot\nabla\bar{\boldsymbol{u}} + \bar{\boldsymbol{u}}\cdot\nabla\boldsymbol{u}' = -\frac{1}{\rho_0}\nabla p' - \frac{\hat{\boldsymbol{z}}g\rho'}{\rho_0} + \nabla\cdot K\nabla\boldsymbol{u}', \tag{2.10}$$

$$\frac{\partial \rho'}{\partial t} + \boldsymbol{u}' \cdot \nabla \bar{\rho} + \bar{\boldsymbol{u}} \cdot \nabla \rho' = \nabla \cdot K \nabla \rho', \tag{2.11}$$

$$\nabla \cdot \boldsymbol{u}' = 0. \tag{2.12}$$

It is now apparent that (2.10)–(2.12) are almost identical to (2.1)–(2.3), with the exception of the cross-terms between the background state and the perturbation variables. Therefore, the existing code which solves (2.1)–(2.3) can be easily adapted to solve for the perturbation quantities in (2.10)–(2.12) using the background (steady) state as a set of input variables. The response to small perturbations introduced into the flow is then calculated using the adapted numerical model. The initial perturbations are typically confined in area, but slowly evolving in time, so as to simulate long waves in the domain.

2.3. *Calculation of eigenmodes*

Simulations of the evolution of perturbations provide some information on the structure of hydraulic control in stratified flows. However, perturbations will inevitably project onto a number of superposed travelling modes, and thus it is not possible to extract information about individual modes. Here we outline an analytical technique to separate the modes available in a turbulent stratified shear flow.

The propagation of waves in inviscid continuously stratified fluids is described by the Taylor–Goldstein equation (see, for example, Banks, Drazin & Zaturska 1976)

$$(\bar{u} - c)(\partial^2 - k^2)\hat{\psi} - \bar{u}_{zz}\hat{\psi} + \frac{N^2}{(\bar{u} - c)}\hat{\psi} = 0, \tag{2.13}$$

where ∂ and z subscripts are used to represent the derivative with respect to z. $N^2 = -g/\rho_0(\partial\bar{\rho}/\partial z)$ is the buoyancy frequency which is non-dimensionalized by a time scale using the channel height and hydraulic velocity scale. The perturbation streamfunction ψ is based on the perturbation velocities, so that

$$u' = \frac{\partial \psi}{z}, \tag{2.14}$$

$$w' = -\frac{\partial \psi}{x}, \tag{2.15}$$

and waves are assumed to be of the form,

$$\psi(x, z, t) = \mathrm{Re}[\hat{\psi}(z)\mathrm{e}^{\mathrm{i}k(x-ct)}]. \tag{2.16}$$

Therefore k is the horizontal wavenumber and c the horizontal phase speed. The Taylor–Goldstein equation describes the behaviour of waves in fluids with shear and stratification and the eigenvalue formulation produces the vertical modal structure ($\hat{\psi}(z)$) as well as the phase speed of waves (c).

The simplest approach to estimating the hydraulic state of a stratified sheared exchange flow would be to extract the vertical profiles of $\bar{u}(z)$ and $\bar{\rho}(z)$ from the background flow. The phase speed of the two lowest modes might then be determined by solving the Taylor–Goldstein equation many times for different profiles at different points in the channel. We would then interpret the flow to be critical at points where one of the two lowest modes has zero phase speed. The difficulty with this approach is that the Taylor–Goldstein equation becomes singular at levels where $\bar{u} - c = 0$ (see Pratt *et al.* 2000 for a more complete description of this problem). Such levels are called critical layers (see, for example, Drazin & Reid 1981), not to be confused with critical points in the context of two-layer hydraulic theory. Near critical layers, the

viscosity and diffusivity, which are neglected by the Taylor–Goldstein equation, play a greater role (Drazin & Reid 1981). In the exchange flow considered here, viscosity and diffusivity play a significant role in determining the flow. This requires the use of a more generalized wave equation originally derived by Koppel (1964). This is the sixth-order viscous stability equation, which can be derived in the same way as the Taylor–Goldstein equation, using (2.1)–(2.3). The stability equation is written as follows:

$$\begin{aligned}-c^2[\partial^2-k^2]\hat{\psi}+c[2\mathrm{i}K_c(\partial^2-k^2)^2+2\bar{u}(\partial^2-k^2)-\bar{u}_{zz}]\hat{\psi}+[K_c^2(\partial^2-k^2)^3\\ -2\mathrm{i}\bar{u}K_c(\partial^2-k^2)^2-2\mathrm{i}\bar{u}_zK_c\partial(\partial^2-k^2)-\bar{u}^2(\partial^2-k^2)\\ +2\mathrm{i}\bar{u}_{zzz}K_c\partial+\bar{u}\bar{u}_{zz}+\mathrm{i}\bar{u}_{zzzz}K_c-N^2]\hat{\psi}=0,\end{aligned} \tag{2.17}$$

where K_c is defined as

$$K_c=\frac{K}{k}, \tag{2.18}$$

and is non-dimensionalized by the factor $(g'H^5)^{1/2}$. K_c can be considered to be a ratio of the time taken for a wave to travel one wavelength, $1/(k(g'H)^{1/2})$, to the time for momentum to diffuse a distance H vertically. As for the underlying simulations, we have assumed a turbulent Prandtl number of unity in all of these calculations. The sixth-order stability equation reduces to the Taylor–Goldstein equation if one removes the effect of viscosity and diffusion by setting $K_c=0$. We can make an immediate simplification to (2.17) by assuming that we are interested in long waves (small wavenumber), so that $k^2\hat{\psi}$ will be small compared to $\partial^2\hat{\psi}$. Therefore we eliminate those terms, simplifying (2.17) to

$$\begin{aligned}-c^2[\partial^2]\hat{\psi}+c[2\mathrm{i}K_c\partial^4+2\bar{u}\partial^2-\bar{u}_{zz}]\hat{\psi}+[K_c^2\partial^6-2\mathrm{i}\bar{u}K_c\partial^4\\ -2\mathrm{i}\bar{u}_zK_c\partial^3-\bar{u}^2\partial^2+2\mathrm{i}\bar{u}_{zzz}K_c\partial+\bar{u}\bar{u}_{zz}+\mathrm{i}\bar{u}_{zzzz}K_c-N^2]\hat{\psi}=0.\end{aligned} \tag{2.19}$$

This problem is reduced to a matrix eigenvalue equation, following the procedure of Winters & Riley (1992) and solved numerically. Start by writing (2.19) as

$$[\mathscr{A}_0+c\mathscr{A}_1-c^2\mathscr{A}_2]\hat{\psi}=0, \tag{2.20}$$

where

$$\mathscr{A}_0=[K_c^2\partial^6-2\mathrm{i}\bar{u}K_c\partial^4-2\mathrm{i}\bar{u}_zK_c\partial^3-\bar{u}^2\partial^2+2\mathrm{i}\bar{u}_{zzz}K_c\partial+\bar{u}\bar{u}_{zz}+\mathrm{i}\bar{u}_{zzzz}K_c-N^2], \tag{2.21}$$

$$\mathscr{A}_1=[2\mathrm{i}K_c\partial^4+2\bar{u}\partial^2-\bar{u}_{zz}], \tag{2.22}$$

$$\mathscr{A}_2=[\partial^2]. \tag{2.23}$$

Linearization of (2.20) (following Winters & Riley 1992) gives

$$\begin{bmatrix}\mathscr{A}_1 & \mathscr{A}_0\\ \mathscr{A}_2 & 0\end{bmatrix}\begin{bmatrix}c\hat{\psi}\\ \hat{\psi}\end{bmatrix}-c\begin{bmatrix}\mathscr{A}_2 & 0\\ 0 & \mathscr{A}_2\end{bmatrix}\begin{bmatrix}c\hat{\psi}\\ \hat{\psi}\end{bmatrix}=0. \tag{2.24}$$

This equation can be solved numerically using the complex analogue of the QZ algorithm (Golub & van Loan 1983; Moler & Stewart 1973).

The equation is solved using the same boundary conditions as the model, with free-slip rigid surfaces at top and bottom. This translates to

$$\hat{\psi}=0,\quad z=0,H, \tag{2.25}$$

and

$$\hat{\psi}_{zz}=0,\quad z=0,H. \tag{2.26}$$

In addition, there is an adiabatic condition on density which imposes the restriction

$$2\hat{\psi}_z\bar{u}_{zzz} = 2(\bar{u}-c)\hat{\psi}_{zzzz} + \mathrm{i}K_c\hat{\psi}_{zzzzzz}, \quad z = 0, H. \tag{2.27}$$

Numerical solutions to (2.24) require vertical profiles of $\bar{u}$ and N^2, and a constant value for K_c. The vertical profiles are taken from the background steady state, with the implicit assumption being that wavelengths are small enough so that the background steady state does not change significantly over one wavelength. A value of K_c requires an estimate of both eddy viscosity and wavenumber. The eddy viscosity is already set in the numerical simulation, however the selection of wavenumber is not so straightforward. The derivation of (2.19) from (2.17) is dependent on long wavelengths, however there will be upper limits on the length of the wave for two reasons. First, if we choose infinitely long waves ($k \to 0$), the parameter K_c will become very large indicating that momentum and density will diffuse so as to significantly alter the waveform over one wavelength. Secondly, the background flow we are investigating is changing with horizontal distance, and therefore we need to select a wavelength over which the flow does not change dramatically. The wavenumber is chosen so that wavelengths are 1/8th of the channel length, resulting in a value of $K_c = 0.003$. We have run additional cases examining the sensitivity to the viscosity parameter and found that the results are not altered by variations in K_c of an order of magnitude.

The solution to (2.24) will then give information about the modes which can exist, and the phase speed (the real part of c) and rates of growth or decay (the imaginary part of c) of those modes. The eigenvectors have a real and imaginary part, and therefore we take the absolute value $((\hat{\psi}\hat{\psi}^*)^{1/2})$ to obtain a simple eigenvector whose structure can be used to identify the lowest modes. The structure and phase speed of vertical mode-1 waves as a function of position in the channel is of primary concern, and will be used to characterize the behaviour of waves in the flow.

3. Results

3.1. *Direct excitation experiments*

Perturbations to the steady exchange shown in figure 3 are applied to a small area ($0.07L \times 0.08H$) on the region of maximum density gradient. The density is perturbed within this region over a dimensionless time of 0.8. This disturbance is designed to stimulate a long mode-1 wave travelling on the density interface, however it is found that results are not particularly sensitive to the length of time, or area over which the perturbation is applied, provided that it is centred on the maximum density gradient.

Figure 4 demonstrates the evolution of a perturbation generated at $x = -0.06$, just to the left of the contraction. The evolution is described by the density variation of the perturbation field on the mid-density isopycnal of the background flow. At any one time this produces the perturbation amplitude as a function of x. Therefore, we combine a number of perturbation amplitude snapshots taken at different times to construct an x, t plot as shown in figure 4. In this plot, one can clearly see the evolution of three different wave extrema. The initial placement of the perturbation produces a positive peak which travels to the left. When the perturbation ends (at dimensionless time 0.8), a trough and a peak remain. The trough propagates to the left at a similar speed to the first peak, while the large peak slowly dissipates, and breaks up into several wave packets travelling to the left and right.

The hydraulic solution for flow with the same reservoir conditions and barotropic

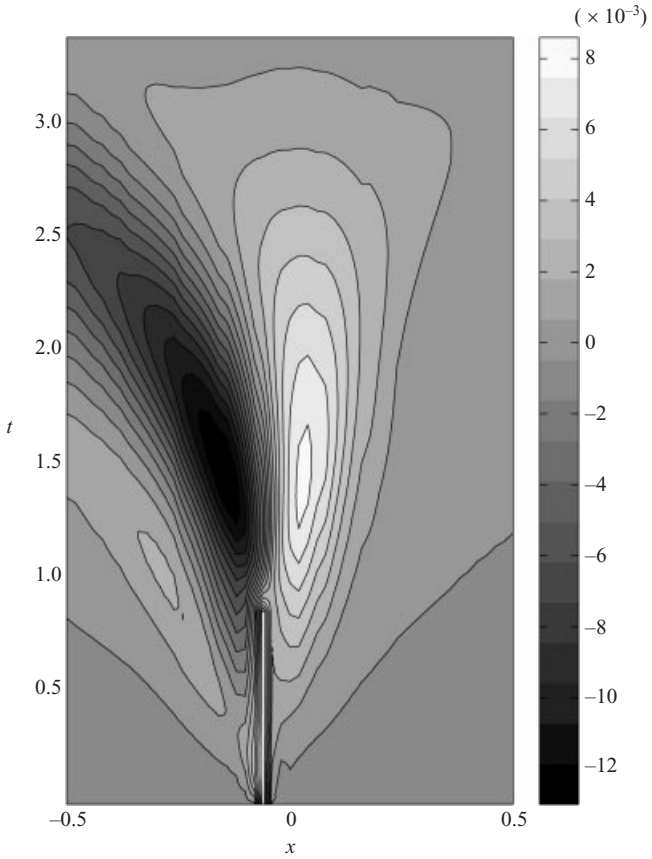

FIGURE 4. Evolution of a linear perturbation in time. Contours show the elevation of the interface from the equilibrium condition in dimensionless units. The perturbation inserted at $x = -0.06$ for time $t = 0.8$ spawns a number of disturbances which mostly travel leftwards (away from the contraction), however some of the disturbance is communicated to the right-hand side of the domain.

flow rate predicts that a wave generated to the left of the contraction cannot propagate information to the right-hand end of the domain. As figure 4 shows, when diffusion is introduced, information propagates to the left, but some adjustment occurs at the right-hand end of the channel, implying that energy is able to leak through. This simulation can be used to infer the speed of propagation of waves as a function of position. The technique used here is simply to identify the position of a peak as a function of time, and find the derivative to give the wave velocity at each point. By exciting a number of perturbations at different positions, the speed of waves at different positions can be calculated. The procedure here is to track wave troughs and peaks as they propagate through the domain, and determine their velocity at each gridpoint. Each dot in figure 5 represents a measured wave velocity at the position shown. Note that there is significant scatter in this data, as the initial perturbation may break into a number of different modes. These modes are compared to the hydraulic prediction of wave speeds, shown as the solid curves. The vertical line is the position of the topographic and virtual controls in the hydraulic solution, which are coincident.

Figure 5 demonstrates that the two-layer hydraulic solution generally overestimates

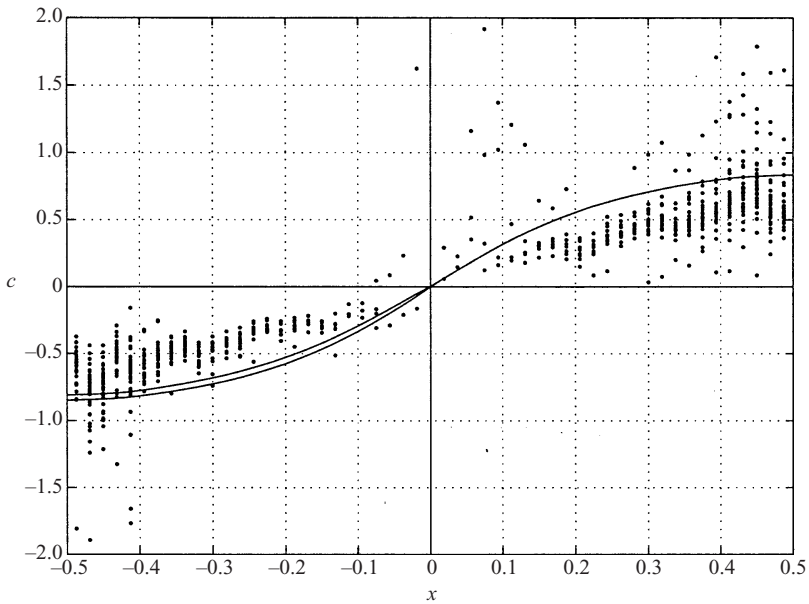

FIGURE 5. Measurements of speed of propagation of disturbances against position for $q_r \approx 1.0$. Each dot represents the speed of one wave, although it is not possible to distinguish the different modes which are created. The two-layer hydraulic prediction of wave speeds is shown as solid curves, with the position of the virtual and topographic control (coincident in this case) shown as a vertical solid line.

the phase speeds which are observed. However, from the point of view of critical flow, it is the direction of wave propagation rather than the phase speed which is of interest. Notably there are no right-going waves ($c > 0$) for $x \lesssim -0.08$, and no left-going modes ($c < 0$) for $x \gtrsim 0$. This implies supercritical flow in the sense that information about interfacial disturbances is not communicated from one end of the channel to the other.

For cases when the barotropic flow rate is finite, two-layer hydraulics predicts that there is some finite subcritical region in the centre of the contraction due to the displacement of the virtual control point. The hydraulic phase speed for a case with $q_r = 4.2$ is shown in figure 6, along with linear perturbation phase speed data using a background flow with the same mixing as in figure 3, but with $q_r \approx 4.2$. Again there are regions of supercritical flow for $x \gtrsim -0.06$ and $x \lesssim -0.28$, implying that there must be some restriction on the propagation of internal waves in these regions. While the position of these control points differs between the hydraulic and the linear perturbation analysis, the end result is that both of these techniques predict that mode-1 interfacial waves are unable to propagate through the channel domain between reservoirs, so that the two reservoirs are isolated from each other.

The propagation of linear disturbances on a background exchange flow demonstrates that while there are differences, the concept of hydraulic control may have relevance to stratified flows where mixing occurs. Qualitative features of hydraulic control appear to be preserved: a subcritical region in the centre of the domain and two supercritical regions on either side. The control points do not occur at the position predicted in the hydraulic solution.

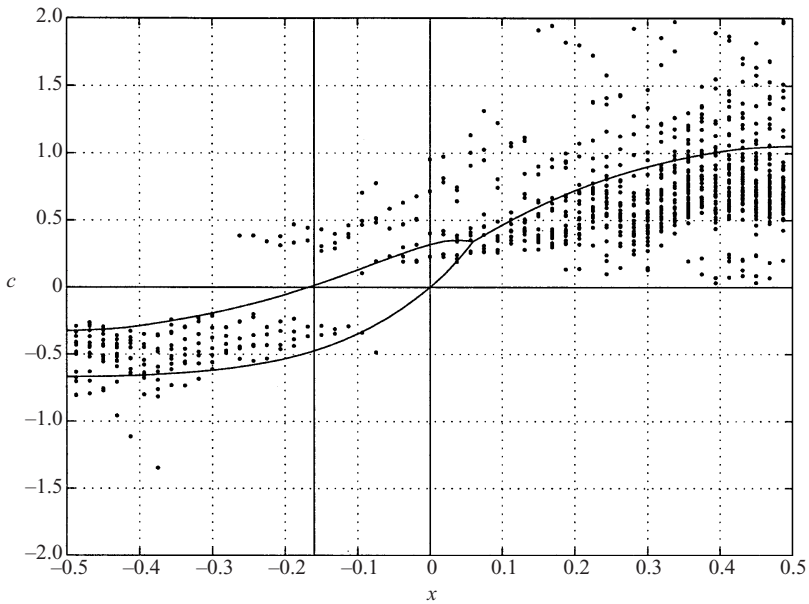

FIGURE 6. Measurements of speed of propagation of disturbances against position for $q_r \approx 4.2$ using the same methodology as figure 5. Virtual and topographic control points predicted by hydraulic theory are shown by vertical lines.

3.2. *Calculation of eigenmodes*

Solutions of (2.24) are sought, with input conditions being vertical profiles of velocity and density from the background states used in the above direct simulation of waves. The numerical solution of this equation produces a large number of modes, and requires significant interpretation to be able to use these results. We assume that the lowest modes (those with a simple eigenvector structure) will be the most important from the point of view of communicating information. In addition, we eliminate modes which are 'trapped' in one layer, so that we predominantly investigate vertical mode-1 waves which are centred on the interfacial region dividing the two-layers. While the instantaneous gradient Richardson number is less than $1/4$ at the interface, the modes we show are stabilized by the effect of viscosity, and thus in all cases the waves are decaying. However the growth or decay is not related to formal definitions of hydraulic control, and therefore we do not specify the imaginary part of the wave speeds.

Figure 7 shows density (a) and velocity profiles (b) at $x = 0$, with eigenvectors of the lowest mode waves (defined to be those modes with only one turning point). The modes shown here are typical of the modes observed at any point in the channel. In panels (c), (e) and (f) we see modes which are trapped in either one of the two-layers, and are propagating in the same direction as the layer velocity. These modes are not of interest to the concept of hydraulic control, as the information which they communicate is by and large related to the portion of the domain which is homogeneous in density and thus irrelevant to the baroclinic flow. Modes shown in (d), (g) and (h) are of greater interest as they are centred on the interfacial region, and thus have the potential to carry information about any possible variation in the main baroclinic state of either reservoir.

The effect of strong shear on the low modes can be seen in figure 7(g, h). Without

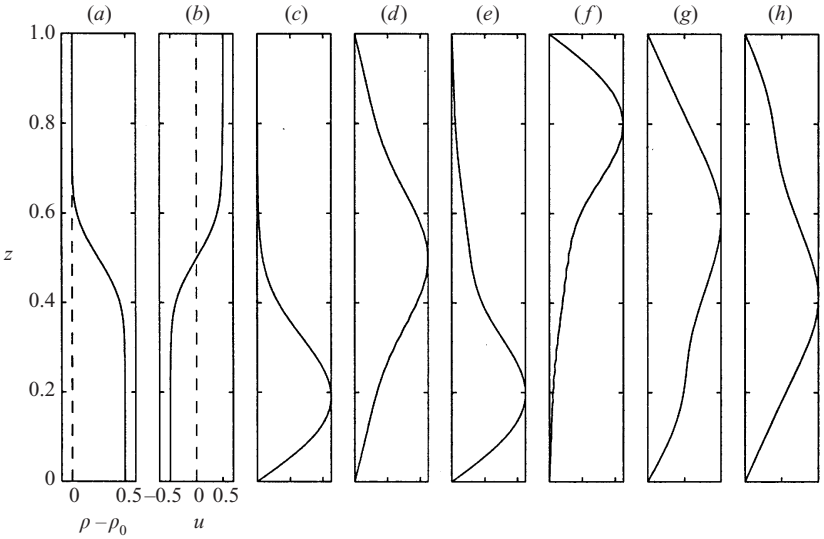

FIGURE 7. Modal structure of selected eigenvectors at $x = 0$ for $q_r \approx 1.0$ as determined by the numerical solution of (2.24). (*a*) Input density profile; (*b*) input velocity profile; (*c*) eigenvector for mode with phase speed $c = -0.61$; (*d*) $c = 0.0013$ (density mode); (*e*) $c = -0.27$; (*f*) $c = 0.28$; (*g*) $c = -0.51$ (vorticity mode); (*h*) $c = 0.51$ (vorticity mode).

shear or viscosity, one would find two mode-1 waves travelling in opposite directions, and the eigenfunction would have a maximum value on the density interface. The addition of viscosity does not significantly alter the velocity or shape of these two waves. However, by incrementally increasing the magnitude of the velocity field, it can be demonstrated that shear distorts these modes so that the mode travelling to the left (figure 7*g*) is skewed upwards, and conversely the mode travelling to the right (figure 7*h*) is skewed vertically downwards. For the purposes of this paper we will call these two modes the *vorticity* modes. The peak of each of the two vorticity modes is coincident with one edge of the interfacial region (the region of maximum curvature in the velocity profile), rather than with the region of maximum density gradient. Mathematically, this result is due to the relative importance of the $\bar{u}_{zz}$ terms (representing the largest vorticity gradients) in (2.24), and demonstrates that the inclusion of shear is crucial in determining the effect of internal modes as carriers of information about the density structure.

There is also a single mode which propagates on the density interface (figure 7*d*) and we therefore refer to this mode as the *density* mode. The density mode is only present when viscosity is finite, and while it is a persistent feature at all points of the channel, it appears to be unaffected by the shear. Instead, the speed of propagation of this mode is best approximated by the velocity of fluid at the mid-isopycnal (see the centre contour in figure 3).

It is possible to track the density mode, as well as the two vorticity modes along the whole channel. On the assumption that these three are the most important mode-1 waves from the point of view of communication of information about stratification, we show the variation of phase speed and modal structure with x in figure 8 ($q_r \approx 1$). Here the dots show the phase speed, while the curved lines show the hydraulic prediction of wave speeds for the case $q_r \approx 1$. At every second gridpoint a panel shows the modal structure of each of the three modes. For the vorticity modes (upper

https://doi.org/10.1017/S0022112001006048 Published online by Cambridge University Press

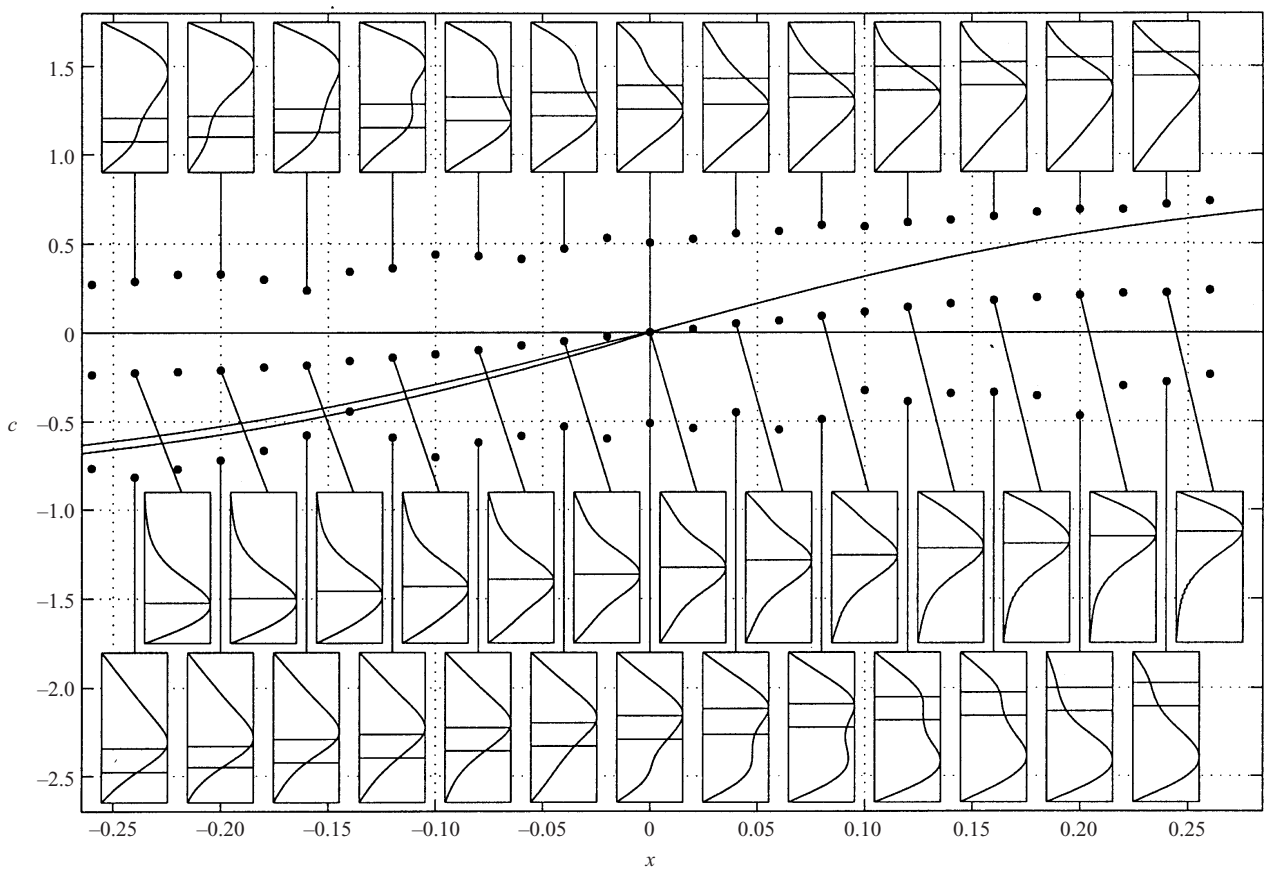

FIGURE 8. Horizontal phase speeds (dots) from the numerical solution of (2.24) for the case $q_r \approx 1$ are plotted against position with hydraulic prediction of wave speeds (solid curves). Panels show details of modal structure for selected waves, with a line joining each panel to the associated wave speed. Within the panel, either the $\bar{u}_{zz}$ extrema is shown by two horizontal lines (top and bottom row of panels), or N^2 maxima is shown by a single horizontal line (central row of panels).

and lower rows of panels) we plot two lines showing the two curvature extrema, and for the density mode (central row of panels) one horizontal line is shown at the maximum of N^2.

Before trying to relate the modes in figure 8 to hydraulic control, it is instructive to use this information to explain the behaviour observed in the numerical simulation of linear waves (§ 3.1). Figure 8 shows very different phase speed information than was obtained in the direct simulation of waves. For example, direct simulation demonstrated that waves generally do not travel to the right from the left-hand side of the channel. Yet the eigenvalue solutions show that modes exist which propagate rightwards at these points. Upon examination of the top row of panels in figure 8 one sees that the rightward travelling vorticity mode undergoes a change on the left-hand side of the domain. As we travel from the centre to the left, a second peak in the eigenvector materialises at $x \approx -0.08$, and at $x \approx -0.12$ the second peak dominates the eigenvector profile. The transition from a vorticity mode to a mode which is trapped in the upper layer is complete at $x \approx -0.20$. This transition is crucial to understanding the results of the direct simulation of linear waves. In the direct simulation, modes are excited by a perturbation centred on the maximum density gradient. At $x \approx -0.24$ (for example), that disturbance at the density interface projects predominantly onto the density mode (which is travelling to the left), and partly onto the leftward propagating vorticity mode. The disturbance will not project significantly onto the rightward travelling vorticity mode. Therefore, while this mode exists, it is not being excited in the linear perturbation experiments. The same argument can be applied to the leftward travelling vorticity mode on the right-hand side of the domain. The wave speeds measured in the perturbation experiments are in general bounded by the density mode and the leftward propagating vorticity mode on the left-hand side of the contraction, and bounded by the density mode and the rightward propagating vorticity mode on the right-hand side of the contraction.

We now consider the implications of the modal structure for hydraulic control. The data of interest in figure 8 pertain to the physical communication of information in the channel which would usually be carried by the baroclinic mode-1 wave. This information is likely to be carried by the density mode, since the maximum of the eigenfunction of this mode is coincident with the interface. The phase speed of the density mode varies along the length of the channel, and is positive on the right-hand side, negative on the left-hand side, and intersects with $c = 0$ at the centre of the contraction. Therefore, this mode is carrying information away from the centre of the contraction. For the density mode, we can specify the critical point to be close to the minimum of the contraction.

The two vorticity modes are also capable of carrying interfacial information, however as the wave propagates there is a progressive transformation in the eigenfunction. A transition occurs at $x \approx -0.1$ for the right travelling mode, and $x \approx 0.1$ for the left travelling mode. The end result is that these modes are capable of carrying interfacial information away from the contraction, but are not effective carriers of interfacial information from the reservoirs towards the contraction. Unlike the density mode which has a definable critical point, their inability to carry information the length of the channel relies upon the gradual evolution of eigenvector shape. However, the vorticity modes do illustrate that interfacial variations in either reservoir will not be able to propagate into the channel.

A feature of hydraulic control is that the position of the virtual control depends upon the barotropic flow rate. This was seen to hold for the direct excitation of waves as shown in figure 6, and we can test if it applies to the eigenvalue analysis using the

https://doi.org/10.1017/S0022112001006048 Published online by Cambridge University Press

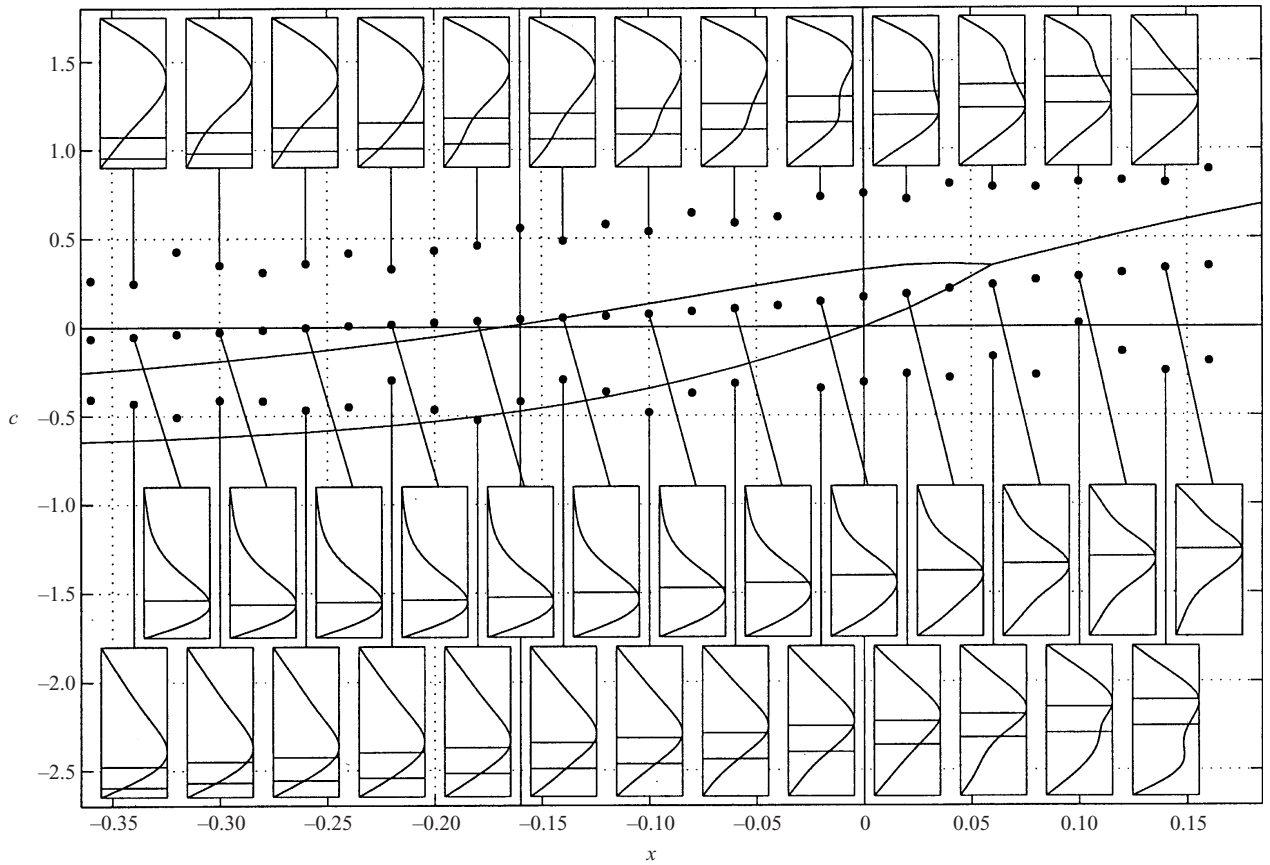

FIGURE 9. As for figure 8, for the case $q_r \approx 4.2$.

case with $q_r \approx 4.2$. Figure 9 shows the density mode, and two vorticity modes for the case with a finite barotropic flow rate, where the field of view has been shifted to the left. Note that the two solid vertical lines show the hydraulic prediction of the virtual and topographic control points from hydraulic theory. The density mode behaves similarly to the zero barotropic flow case, and the phase speed intersects with zero at $x \approx -0.25$. This is consistent with the observation that waves cannot travel to the right for $x \lesssim -0.28$ in the direct simulation of waves (see figure 6). It is notable that hydraulic theory predicts the position of the virtual control at $x \approx -0.16$ in this case. This may imply that the zero crossing of the density mode may represent an analogy to the hydraulic virtual control point, however the analogy is not complete, because the density mode only appears when viscosity is finite, and thus cannot be part of the two-layer inviscid hydraulic solution.

The behaviour of the vorticity modes presents a different picture in this case. A transition occurs at $x \approx 0.2$ (not shown) for the leftward vorticity mode, and at $x \approx 0$ for the rightward vorticity mode. As was the case with no barotropic flow rate, this indicates that reservoir-to-reservoir communication will not be possible via the vorticity modes. One might claim that the rightward vorticity mode transition at $x \approx 0$ represents a topographic control. However the case for the leftward vorticity mode transition as a virtual control region is weak, as it is on the opposite side of the contraction to the predicted hydraulic virtual control.

4. Discussion and conclusions

Two different methods of evaluating the behaviour of linear internal waves in exchange flows have been demonstrated. The first method relates to the direct simulation of linear perturbations by solving (2.10)–(2.12) using an adaptation of the numerical model S-FIT. The second method uses the solution of the sixth-order stability equation to find both the phase speed and modal structure of waves. The direct simulation method considers all available modes which are excited by an initial disturbance, whereas the second method produces a large number of modes which are subjectively assessed, to determine which are the important modes. The techniques reveal different but complementary information about the propagation of low-mode internal waves through exchange flows. Both show that, as in two-layer flows, control may be thought of in terms of information propagation. More precisely, it is the propagation of information regarding the vertical location of the maximum density gradient that is important.

The eigenvalue method is perhaps the more useful of the two approaches as it gives the modal structure at any point, and requires only profiles of velocity and density, and estimates of the turbulent eddy viscosity and wavenumber. A single mode, centred on the maximum density gradient, appears to conform to the behaviour of the interfacial mode in two-layer theory. It is the intersection of the phase speed with zero which indicates the position of a control in the flow. The control point shifts upstream relative to the barotropic flow as barotropic flow rate increases, indicating that this control point may be analogous to the virtual control point identified in hydraulic theory.

There are two other important modes, which have a maximum near the interface, but are skewed from the interface so that the maximum in the eigenvector coincides with the maximum vorticity gradients. While neither of these modes has zero phase speed, the vorticity modes can nonetheless be used to infer details about control. In this case, the mode undergoes a transition so that upstream of the transition (relative to the

direction of travel of the wave) the eigenfunction peak is not in the interfacial region. This implies that the mode is an ineffective carrier of interfacial information upstream of the transition point. Conversely, downstream of the transition, the vorticity mode takes a form which indicates it could be an effective carrier of interfacial information. In one sense this can be considered to result in control of the flow of information, however this is a different concept from hydraulic control, as the transition occurs gradually and thus instead of a critical point at which wave speeds are zero we find a critical region over which control gradually takes effect. In any case, this results in the same conclusion: that the system is in a state where end conditions can change without altering the flow.

There are implications in these findings for the extension of hydraulic control to cases with continuous stratification and mixing. Two primary features of hydraulic control outlined in §1 are first that local information (at a control point) can be extrapolated to give global information, and secondly that the hydraulic solution gives an upper bound on flux through the channel. Extrapolation of global information from local variables is difficult in cases where mixing is significant, since energy is continually being lost to mixing. However, the above analysis demonstrates that in stratified exchange flows, reservoir conditions can be altered without affecting the flow. Thus it is possible that a solution may exist which can be used to place an upper bound on the flux for a given rate of mixing.

Another application of this work is in the analysis of geophysical field data to determine whether flows are supercritical. This may have relevance to both uni-directional flows (for example, abyssal flow over mid-ocean ridges) and bi-directional flows (such as the Bosphorus). In the case of uni-directional flow, control points indicate that downstream conditions may vary without altering the flux. In such cases it may be possible to calculate flux with only limited knowledge of the downstream conditions. Alternatively, if it can be determined that bi-directional exchange flow is controlled, then the implication is that changes to one reservoir may not affect the other reservoir. For example, profiles of velocity and density at discrete locations taken from field measurements such as Gregg & Özsoy (2001) may be used to calculate the eigenvalue solution to the viscous stability equation. By selecting the lowest modes from the solution, it may be possible to determine whether the flow is controlled, and if so, which parts of the channel are super- and subcritical. This can be used to predict flux variations due to changes in external conditions.

Thanks to Larry Redekopp for his assistance in understanding the behaviour of waves in these flows. Graham Hughes and Ross Griffiths also helped with the direction of this work. Three anonymous referees provided useful and thoughtful comments which contributed to substantial improvements to the manuscript. The first author was supported by an Australian Postgraduate Award and Jean Rogerson Postgraduate Supplementary Scholarship, and the second author was supported by ONR support grant number N0014-92-J1180 for the duration of this work.

REFERENCES

Armi, L. 1986 The hydraulics of two flowing layers with different densities. *J. Fluid Mech.* **163**, 27–58.

Armi, L. & Farmer, D. M. 1986 Maximal two-layer exchange through a contraction with barotropic net flow. *J. Fluid Mech.* **164**, 27–51.

Baines, P. G. 1995 *Topographic Effects in Stratified Flows.* Cambridge University Press.

Banks, W. H. H., Drazin, P. G. & Zaturska, M. B. 1976 On the normal modes of parallel flow of an inviscid stratified fluid. *J. Fluid Mech.* **75**, 149–171.

Dalziel, S. B. 1991 Two layer hydraulics: a functional approach. *J. Fluid Mech.* **223**, 135–163.

Drazin, P. G. & Reid, W. H. 1981 *Hydrodynamic Stability*. Cambridge University Press.

Engqvist, A. 1996 Self-similar multi-layer exchange flow through a contraction. *J. Fluid Mech.* **328**, 49–66.

Golub, G. H. & van Loan, C. F. 1983 *Matrix Computations*. John Hopkins University Press.

Gregg, M. C. & Özsoy, E. 2001 Flow, water mass changes, and hydraulics in the Bosphorus. *J. Geophys. Res.* In press.

Hogg, A. M., Ivey, G. N. & Winters, K. B. 2001 Hydraulics and mixing in controlled exchange flows. *J. Geophys. Res.* **103** (C1), 30695–30711.

Koppel, D. 1964 On the stability of a thermally stratified fluid under the action of gravity. *J. Meth. Phys.* **5**, 963–982.

Lawrence, G. A. 1990 On the hydraulics of Boussinesq and non-Boussinesq two-layer flows. *J. Fluid Mech.* **215**, 457–480.

Moler, C. B. & Stewart, G. W. 1973 An algorithm for generalized matrix eigenvalue problems. *SIAM J. Numer. Anal.* **10**, 241–256.

Pratt, L. J., Deese, H. E., Murray, S. P. & Johns, W. 2000 Continuous dynamical modes in straits having arbitrary cross sections with applications to the Bab al Mandab. *J. Phys. Oceanogr.* **30**, 2515–2534.

Pratt, L. J., Johns, W., Murray, S. P. & Katsumata, K. 1999 Hydraulic interpretation of direct velocity measurements in the Bab al Mandab. *J. Phys. Oceanogr.* **29**, 2769–2784.

Winters, K. B. & Riley, J. J. 1992 Instability of internal waves near a critical level. *Dyn. Atmos. Oceans* **16**, 249–278.

Winters, K. B. & Seim, H. E. 2000 The role of dissipation and mixing in exchange flow through a contracting channel. *J. Fluid Mech.* **407**, 265–290.

Winters, K. B., Seim, H. E. & Finnigan, T. D. 2000 Simulation of non-hydrostatic, density-stratified flow in irregular domains. *Intl J. Numer. Meth. Fluids* **32**, 263–284.

Wood, I. R. 1968 Selective withdrawal from a stably stratified fluid. *J. Fluid Mech.* **32**, 209–223.

Wood, I. R. 1970 A lock exchange flow. *J. Fluid Mech.* **42**, 671–687.